

# PCCP

Accepted Manuscript



This is an *Accepted Manuscript*, which has been through the Royal Society of Chemistry peer review process and has been accepted for publication.

*Accepted Manuscripts* are published online shortly after acceptance, before technical editing, formatting and proof reading. Using this free service, authors can make their results available to the community, in citable form, before we publish the edited article. We will replace this *Accepted Manuscript* with the edited and formatted *Advance Article* as soon as it is available.

You can find more information about *Accepted Manuscripts* in the [Information for Authors](#).

Please note that technical editing may introduce minor changes to the text and/or graphics, which may alter content. The journal's standard [Terms & Conditions](#) and the [Ethical guidelines](#) still apply. In no event shall the Royal Society of Chemistry be held responsible for any errors or omissions in this *Accepted Manuscript* or any consequences arising from the use of any information it contains.

## Depletion region effect of highly efficient hole conductor free $\text{CH}_3\text{NH}_3\text{PbI}_3$ perovskite solar cells

Sigalit Aharon, Shany Gamliel, Bat El Cohen, Lioz Etgar\*

The Hebrew University of Jerusalem, Institute of Chemistry, Casali Center for Applied Chemistry

\*E-mail: [lioz.etgar@mail.huji.ac.il](mailto:lioz.etgar@mail.huji.ac.il)

KEYWORDS: Perovskite, depletion layer, solar cells, blocking layer, hole conductor

### Abstract

Inorganic-organic perovskite is currently attracting lot of attention due to its use as a light harvester in solar cells. The large absorption coefficients, high carrier mobility and good stability of organo-lead halide perovskites present good potential for their use as light harvesters in mesoscopic hetero-junction solar cells. This work concentrated on a unique property of the lead halide perovskite, its function simultaneously as light harvester and hole conductor in the solar cell. A two-step deposition technique was used to optimize the perovskite deposition and to enhance the solar cell efficiency. It was revealed that the photovoltaic performance of the hole conductor free perovskite solar cell is strongly dependent on the depletion layer width which was created at the  $\text{TiO}_2/\text{CH}_3\text{NH}_3\text{PbI}_3$  junction. X-ray diffraction measurements indicate that there were no changes in the crystallographic structure of the  $\text{CH}_3\text{NH}_3\text{PbI}_3$  perovskite over time, which supports the high stability of these hole conductor free perovskite solar cells. Furthermore, the power conversion efficiency of the best cells reached 10.85% with a fill factor of 68%,  $V_{oc}$  of 0.84V, and  $J_{sc}$  of 19  $\text{mA}/\text{cm}^2$ , the highest efficiency to date of a hole conductor free perovskite solar cell.

## Introduction

The search for alternative energy solutions is currently a leading research area and will remain so for the foreseeable future, and photovoltaics (PV) are a key technology for a sustainable energy supply. The basic requirement from PV devices is the charge separation of electrons and holes in a material, which absorb the light, and the conductivity of these charges to different contacts.

A recent breakthrough was made by using new light absorber, the inorganic-organic perovskite, in the solar cell. The inorganic-organic perovskite consists of inorganic part, usually a metal divalent cation to satisfy the charge balancing. The organic part consists of organic cation to derive the three-dimension perovskite structure.

The inorganic-organic perovskite has a direct band gap, large absorption coefficients<sup>1</sup> and high carrier mobility,<sup>2,3</sup> which presents good potential for its use as light harvesters in mesoscopic hetero-junction solar cells.

Several studies used  $\text{CH}_3\text{NH}_3\text{PbI}_3$  perovskite as sensitizers in photoelectrochemical cells with liquid electrolyte<sup>4,5,6</sup>. However, the performance of these systems rapidly declined due to dissolution of the perovskite. This problem was solved by replacing the electrolyte with a solid state hole conductor.<sup>7</sup> Moreover, the tin iodide-based perovskite  $\text{CsSnI}_3$  has been employed as a hole conductor together with N719 as a sensitizer in solid state dye-sensitized solar cells, yielding a power conversion efficiency (PCE) of 8.5%.<sup>8</sup> Several reports showed<sup>9,10,11</sup> efficient hybrid organic-inorganic solar cells, based on meso-superstructured organo-halide perovskite, yielding power conversion efficiency of 10.9% to 12.3%.

A high open circuit voltage was demonstrated in these perovskite based solar cells, having  $V_{oc}$  of 1.15 V and 1.3 V<sup>12,13</sup>. Recently impedance spectroscopy was carried out on these high efficiency perovskite solar cells, the authors recognized charge accumulation in the absorber material (the perovskite) which derive from the capacitance of the devices<sup>14</sup>. Good correlation between the calculated electronic and optical band gap and the experimental results was found using theoretical modeling of the perovskites based halides<sup>15</sup>. In addition, the high efficiency achieved for the perovskite based solar cells was supported by measuring long-range electron-hole diffusion length<sup>16,17</sup>.

Recently, more than 15% power conversion efficiency was reported. In one work two step deposition technique of the perovskite was demonstrated<sup>18</sup> while in other work co-evaporation deposition technique on flat surface was used<sup>19</sup>. Besides this breakthrough, Etgar et al.<sup>20</sup> reported on the use of hole conductor free perovskite solar cells. The authors demonstrated for the first time that the

perovskite can function as light harvester and as hole conductor at the same time. In early work 5% efficiency was reported and recently this performance was improved to 8% efficiency for depleted hole conductor free perovskite solar cells<sup>21</sup>. In addition a PCE of 10.49% was achieved for hole conductor free perovskite solar cell<sup>22</sup>. Elimination of hole conductor can improve the stability, lower the cost and simplify the fabrication process.

In this research, we concentrated on using  $\text{CH}_3\text{NH}_3\text{PbI}_3$  perovskite as a light harvester and as a hole conductor simultaneously in the solar cell. We performed a complete study of several parameters, which influence the PV performance of these hole conductor free lead halide iodide perovskite solar cells. We optimized the use of two-step deposition technique of the perovskite, and we have found a correlation between the depletion layer width at the  $\text{TiO}_2/\text{CH}_3\text{NH}_3\text{PbI}_3$  junction and the power conversion efficiency observed. X-Ray diffraction analysis revealed that there is no change in the crystallographic structure of the  $\text{CH}_3\text{NH}_3\text{PbI}_3$  perovskite over time, indicating the high stability of these cells. Finally, the best power conversion efficiency (PCE) achieved in this work was 10.85%, the highest efficiency to date of a hole conductor free perovskite solar cell.

## Results and discussion

This work concentrates on the use of lead halide perovskite as a light harvester and as a hole conductor simultaneously in the solar cell. The solar cell structure and its energy level diagram is shown in figure 3A and 3B respectively, which consists of a blocking layer following by the deposition of mesoporous  $\text{TiO}_2$  film, perovskite film and gold as the back contact. The blocking layer has an important role as it improves the PV parameters of the solar cell. In this work, the blocking layer was fabricated by spin coating a solution of diluted titanium diisopropoxidebis(acetylacetonate) (TiDIP) in ethanol, which permitted more control of the blocking layer thickness and density. The influence of the blocking layer on the PV performance was investigated by changing the blocking layer thickness and concentration. Table 1 presents the PCE of cells made in different blocking layer conditions (spin velocity (round per minute (rpm)) and the TiDIP precursor concentration). In order to study the influence of the blocking layer conditions on the PV performance all the other parameters were held constant.

The best PCE was observed for spin velocity of 1500 rpm and 0.15% volume fraction of TiDIP in the blocking layer conditions. Looking at the results, it was observed that for each concentration, there is an optimal spin velocity. At low concentrations, the best efficiency was observed at low spin velocity. The spin velocity determines the blocking layer thickness, so when using low TiDIP

concentration, a thick blocking layer is preferred (i.e. low spin velocity). On the other hand, at a high concentration of TiDIP, the best efficiency was observed at the high spin velocity. The high spin velocity enables achieving a thin, uniform blocking layer, so that a high TiDIP concentration can be used. In the case of high TiDIP concentration and low spin velocity, a thick and condensed blocking layer was formed resulting in low PV performance.

**Table 1:** Efficiencies of the hole conductor free perovskite solar cells at different blocking layer conditions, i.e. spin velocity (rpm) and at various TiDIP concentrations.

Volume fraction of TiDIP (%)	Spin Velocity 500 rpm	Spin Velocity 1500 rpm	Spin Velocity 2500 rpm
0.05	4.5%	3.0 %	3.0%
0.10	4.2%	7.0%	2.0%
0.15	5.0%	7.2%	2.2%
0.20	3.0%	5.4%	6.5%

The deposition of the lead halide iodide perovskite on the mesoporous TiO<sub>2</sub> was done based on the two-step deposition method (spin & dip) described earlier<sup>18</sup> but with several modifications which assist in controlling the lead halide iodide perovskite deposition on the mesoporous TiO<sub>2</sub>. The first step was spinning PbI<sub>2</sub> on the mesoporous TiO<sub>2</sub> film and annealing at 70°C, while the second step was dipping the PbI<sub>2</sub> electrode into CH<sub>3</sub>NH<sub>3</sub>I solution. After the PbI<sub>2</sub> reacts with the CH<sub>3</sub>NH<sub>3</sub>I, the CH<sub>3</sub>NH<sub>3</sub>PbI<sub>3</sub> was formed. An important step in this deposition technique is the wait time period after dropping the PbI<sub>2</sub> on the mesoporous TiO<sub>2</sub> film, before spinning. We investigated the wait time parameter and observed its influence on the PV parameters of these cells. The results are summarized in figure 1. The highest efficiency (8.0%) was achieved at a wait time of 3 minutes.

During 3 minutes of waiting time, the PbI<sub>2</sub> creates a uniform coating on the mesoporous TiO<sub>2</sub> surface while a longer waiting time (5 min) causes evaporation of the PbI<sub>2</sub>'s solvent, which could create a non-uniform coating of the PbI<sub>2</sub> on the mesoporous TiO<sub>2</sub> surface. Conversely, the coverage of the surface by PbI<sub>2</sub> isn't complete during a too-short wait time.

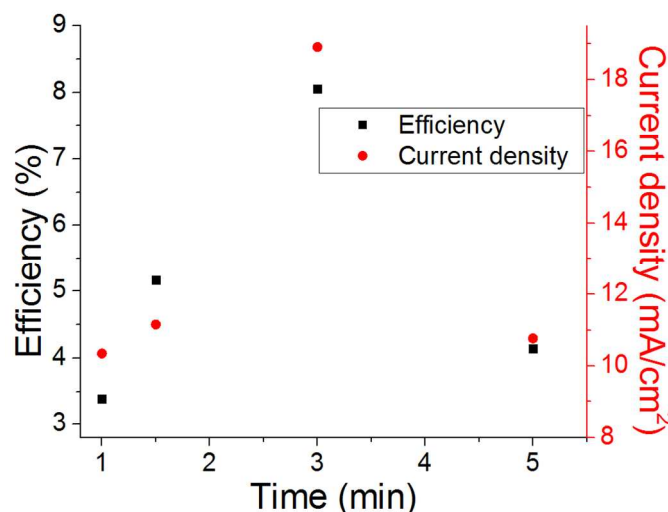


**Figure 1:** The current density and the efficiency of the cells versus the wait time (min) between dropping the  $\text{PbI}_2$  until the beginning of the spinning.

The influence of the  $\text{TiO}_2$  film thickness was investigated by making hole conductor free perovskite based solar cells using different thickness of mesoporous  $\text{TiO}_2$  films while keeping the  $\text{CH}_3\text{NH}_3\text{PbI}_3$  perovskite film thickness constant (same deposition parameters were used for the perovskite deposition). To achieve different  $\text{TiO}_2$  film thicknesses, the  $\text{TiO}_2$  paste was diluted by ethanol at various ratios. The various dilutions produced different thicknesses of  $\text{TiO}_2$  films as seen in figures 2A-E. The thickness of the mesoporous  $\text{TiO}_2$  film was measured by the Dektak 150 profiler, and the results are shown in the figure 2E graph. Figure 2A-D presents extra high resolution scanning electron microscopy (XHR-SEM) of the various  $\text{TiO}_2$  thicknesses in the complete set of thicknesses of  $\text{TiO}_2/\text{CH}_3\text{NH}_3\text{PbI}_3$  perovskite solar cells. It can be observed that the  $\text{CH}_3\text{NH}_3\text{PbI}_3$  formed an over layer on top of the  $\text{TiO}_2$  film. Probably some of the  $\text{CH}_3\text{NH}_3\text{PbI}_3$  is penetrated into the  $\text{TiO}_2$  film, however the thick over layer of the  $\text{CH}_3\text{NH}_3\text{PbI}_3$  film ( $300\text{nm}\pm 50\text{nm}$ ) indicates that most of the perovskite is staying on top of the  $\text{TiO}_2$  film. Table 2 summarizes the results obtained for the solar cells made with various  $\text{TiO}_2$  thicknesses. For each  $\text{TiO}_2$  thickness more than 5 cells were fabricated in order to investigate the reliability of the presented results. The highest efficiency was observed for cells made with mesoporous  $\text{TiO}_2$  film of  $620\pm 25\text{nm}$  thickness. In these cells, the current density and the open circuit voltage were higher than the other cells made with different thicknesses of  $\text{TiO}_2$ . The lowest efficiencies were observed for the thick  $\text{TiO}_2$  film ( $750\pm 25\text{nm}$ ) and for the thin  $\text{TiO}_2$  film ( $400\pm 25\text{nm}$ ). In addition, the FF and the current density for these cells were also the lowest compared with the other  $\text{TiO}_2$  thicknesses.



**Table 2:** PV performance of the hole conductor free  $\text{TiO}_2/\text{CH}_3\text{NH}_3\text{PbI}_3$  perovskite based solar cells obtained for various  $\text{TiO}_2$  film thicknesses.

Thickness of $\text{TiO}_2$ film (nm) $\pm 25\text{nm}$	$V_{oc}$ (V)	$J_{sc}$ ( $\text{mA}/\text{cm}^2$ )	FF	Efficiency (%)
750	0.66	12.47	0.45	3.7
620	0.73	16.03	0.61	7.2
450	0.68	13.27	0.63	5.7
400	0.65	10.47	0.55	3.8

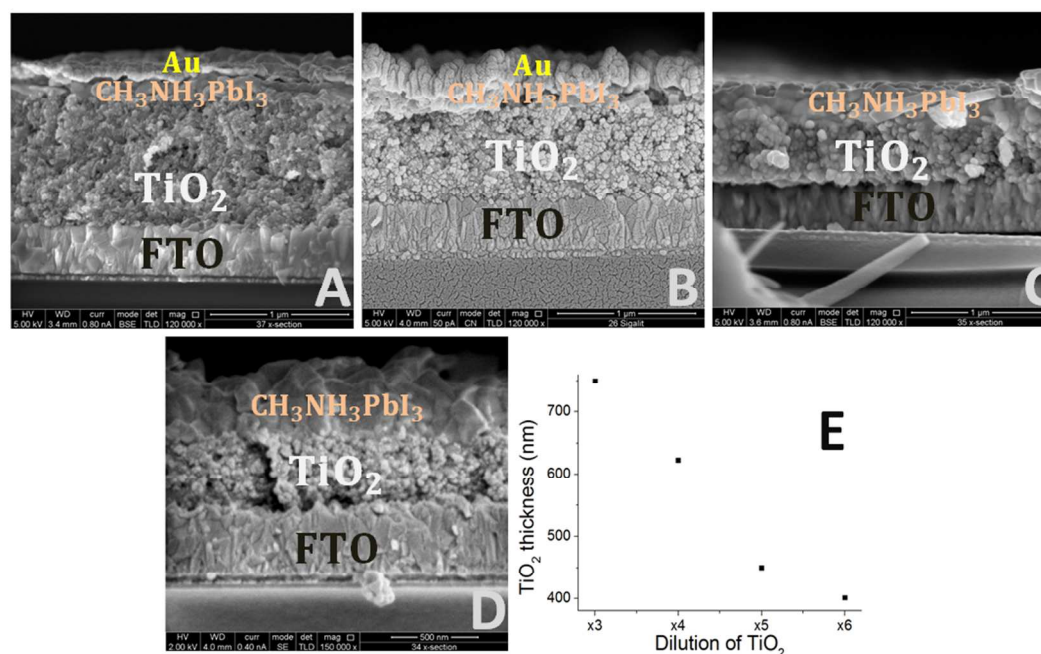


**Figure 2:** XHR-SEM of the different  $\text{TiO}_2$  thickness in the complete  $\text{TiO}_2/\text{CH}_3\text{NH}_3\text{PbI}_3$  perovskite based solar cells. (A) The thicker  $\text{TiO}_2$  film corresponds to 3 times dilution see figure 2E. (B) 4 times dilution. (C) 5 times dilution. (D) 6 times dilution. Importantly the thickness was measured by surface profiler which its results are shown in figure 2E.

To understand the reason for the difference in PV performance observed when using a variety of  $\text{TiO}_2$  film thicknesses, capacitance voltage measurements were performed. In our previous work,<sup>21</sup> it was reported that a depletion layer is created in the  $\text{CH}_3\text{NH}_3\text{PbI}_3$  perovskite film and in the  $\text{TiO}_2$  mesoporous film. This depletion layer assists in the charge separation and inhibits the back reaction of electrons from the  $\text{TiO}_2$  to the  $\text{CH}_3\text{NH}_3\text{PbI}_3$  film. To estimate the depletion region width, Mott Schottky analysis<sup>23</sup> on the  $\text{TiO}_2/\text{CH}_3\text{NH}_3\text{PbI}_3$  heterojunction solar cells was performed.

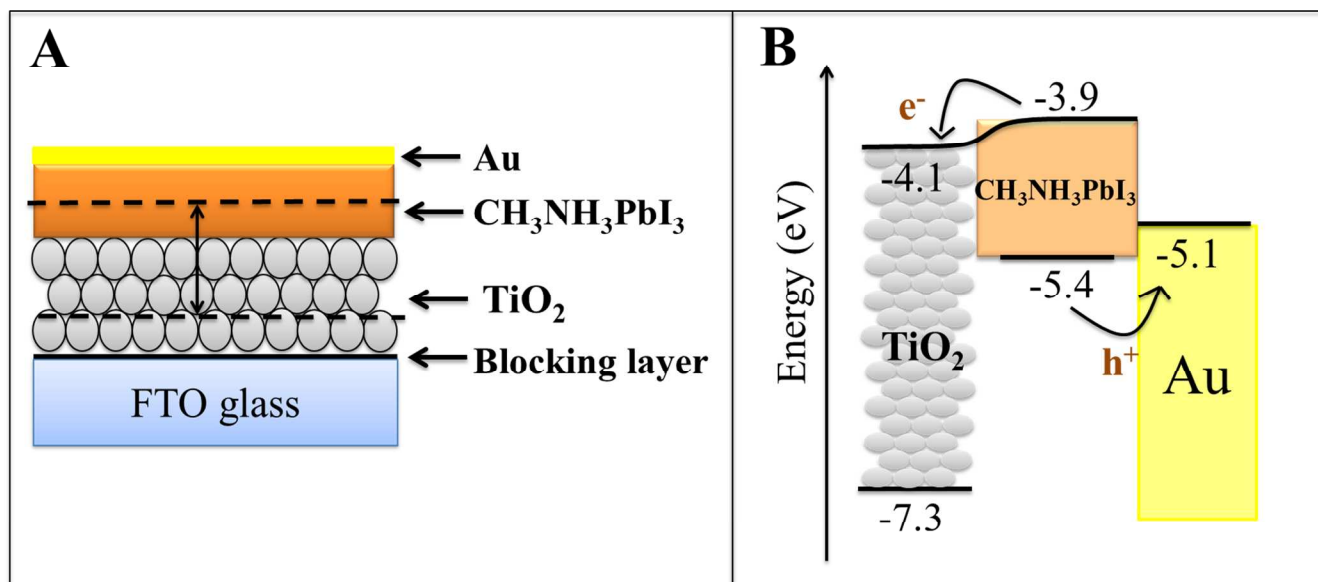


**Figure 3:** (A) The structure of the hole conductor free  $\text{TiO}_2/\text{CH}_3\text{NH}_3\text{PbI}_3$  perovskite based solar cells. The arrow indicates the depletion region observed at the  $\text{TiO}_2/\text{CH}_3\text{NH}_3\text{PbI}_3$  junction. (B) Energy level diagram of the discussed solar cell which shows the charge separation process. The position of the energy levels are taken from ref. 20.

The capacitance at the junction which described in equation 1 is calculated from the depletion approximation<sup>24</sup>. The depletion approximation implies that there are no free carriers in the space charge region at the junction under investigation.

$$(1) \frac{1}{C^2} = \frac{2}{\epsilon \epsilon_0 q A^2 N} (V_{bi} - V)$$

where  $C$  is the measured capacitance,  $A$  is the active area,  $V$  is the applied bias,  $\epsilon$  is the static permittivity,  $\epsilon_0$  is the permittivity of free space,  $q$  is elementary charge and  $N$  is the doping density of the donor. The static permittivity of  $\text{CH}_3\text{NH}_3\text{PbI}_3$  was measured and calculated to be  $30^{25,26}$ . From the slope of the Mott Schottky plot in the linear regime, the net doping density of the  $\text{CH}_3\text{NH}_3\text{PbI}_3$  film can be calculated. Moreover, the intersection of the linear regime in the Mott Schottky plot with the x-axis determines the built-in voltage, which suppressed the back reaction of electrons from the  $\text{TiO}_2$  film to the  $\text{CH}_3\text{NH}_3\text{PbI}_3$  film.

The depletion width is calculated according to:<sup>27</sup>

$$(2) W_{p,n} = \frac{1}{N_{a,d}} \sqrt{\frac{2\epsilon V_{bi}}{q(N_a + N_d)}}$$



where  $N_a$  and  $N_d$  are the doping density of the acceptor and the donor, respectively. Literature values for doping density in nanoporous  $\text{TiO}_2$  start at  $N_a=1 \times 10^{16} \text{ cm}^{-3}$ .<sup>28,29,30</sup>

Table 3 summarizes the calculated  $W_n$ ,  $W_p$ , total depletion width ( $W_t$ ) and the built-in potential ( $V_{bi}$ ) for the various  $\text{TiO}_2$  film thicknesses.

**Table 3:** Calculated depletion width and the built-in potential for various  $\text{TiO}_2$  film thicknesses.

\* The “depleted  $\text{TiO}_2$ ” is the fraction of the part in the  $\text{TiO}_2$  film that is depleted.

Thickness of $\text{TiO}_2$ (nm) $\pm 25$ nm	Depleted $\text{TiO}_2^*$	$V_{oc}$ (V)	$V_{bi}$ (V)	Efficiency (%)	$W_t$ (nm)	$W_n$ (nm)	$W_p$ (nm)
750	0.12	0.66	0.87	3.8	223	88	135
620	0.49	0.73	0.74	7.2	395	306	89
450	0.31	0.68	0.70	5.7	239	140	99
400	0.10	0.65	0.73	3.7	194	44	150

\* More than 5 cells were fabricated for each condition.

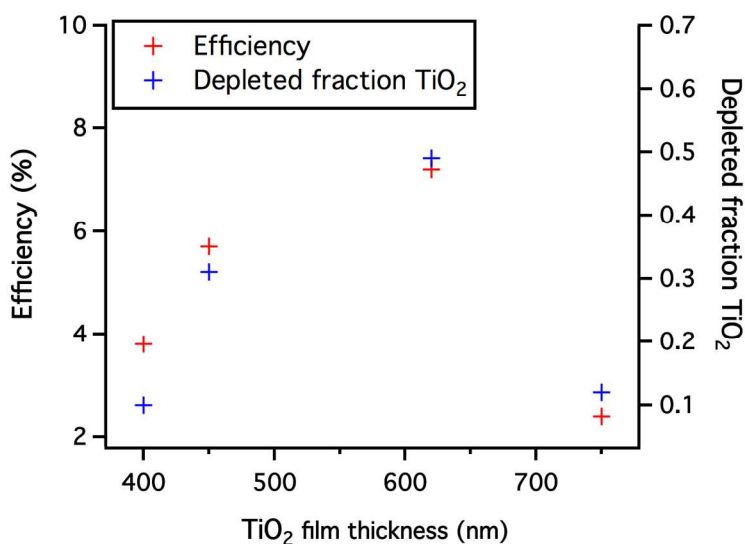
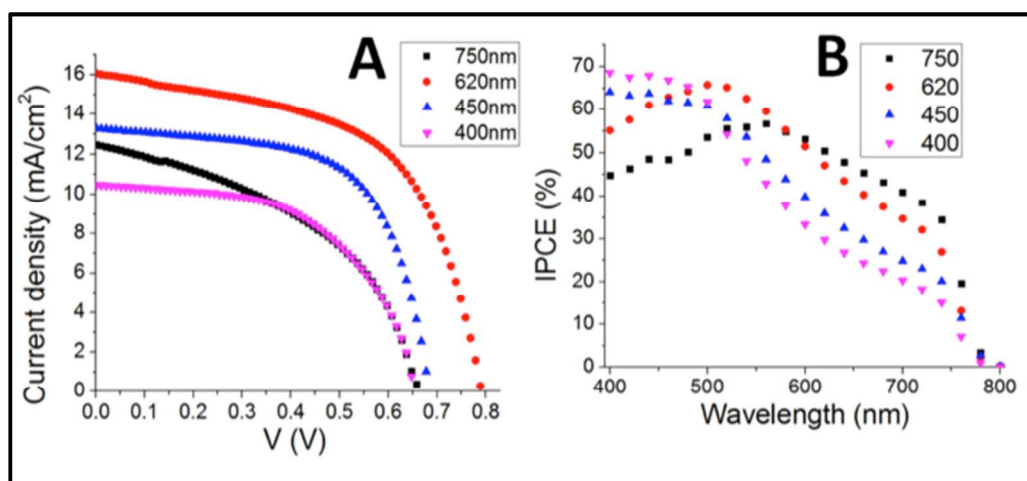


**Figure 4:** Efficiency and depleted fraction of the  $\text{TiO}_2$  as a function of the  $\text{TiO}_2$  film thickness.

The correlation between the power conversion efficiency for the various  $\text{TiO}_2$  film thicknesses and the depleted fraction of the  $\text{TiO}_2$  film can be observed in figure 4. In the case of the highest efficiency, the total depletion width ( $W_t$ ) is the maximum and equals 395nm; moreover, half of the  $\text{TiO}_2$  film is depleted (depleted fraction equals to 0.49), suggesting that the depletion region indeed

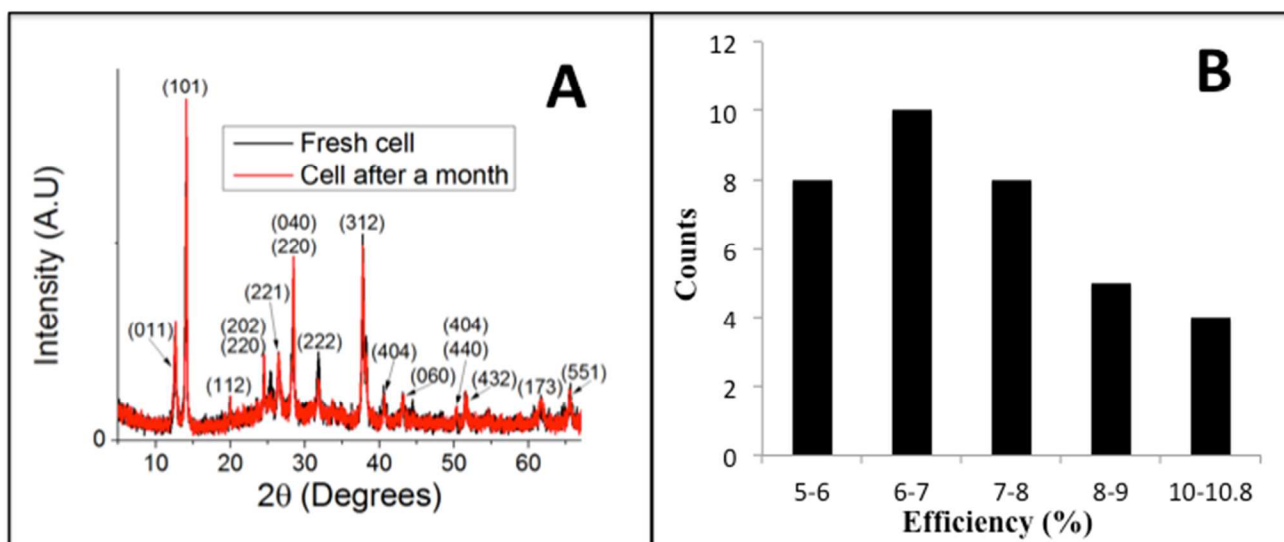
assists in the charge separation and suppresses the back reaction, and consequently contributes to the increase in the power conversion efficiency of the cells. For the low efficiencies, the  $W_t$  is the lowest, and the depleted fraction of the  $\text{TiO}_2$  is around 0.1, which means that only 10% of the total  $\text{TiO}_2$  thickness is depleted. Further, there is good agreement between the open circuit voltage and the built-in potential observed from the Mott Schottky plot. As a conclusion there is a very good agreement between the depletion region width and the PCE observed.

The JV curves and the incident photon to current efficiency (IPCE) of the hole conductor free perovskite solar cells using various  $\text{TiO}_2$  film thicknesses are presented in figures 5A and 5B.



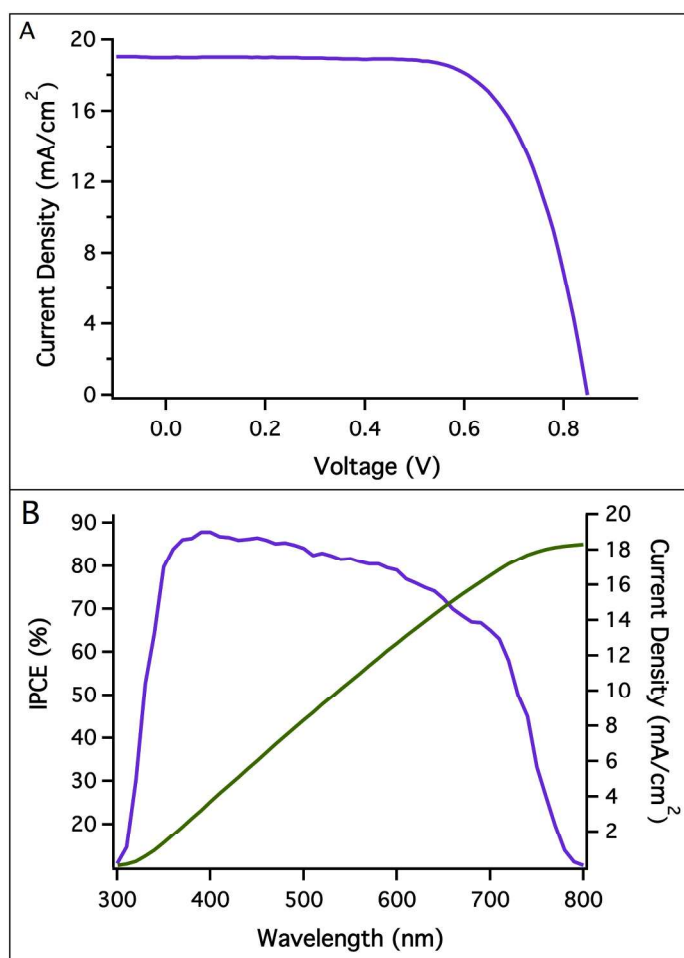
**Figure 5:** (A) JV curves of the different  $\text{TiO}_2$  film thickness for the hole conductor free perovskite solar cells and their (B) IPCE spectra.

Figure 6A presents XRD diffraction of a fresh cell and the same cell (which stayed in the dark) after a month; the peaks in the figure are indexed according to ref. 25, while two third of the peaks belong to the Orthorhombic structure of the  $\text{CH}_3\text{NH}_3\text{PbI}_3$  perovskite, and one third belongs to the tetragonal structure of the  $\text{CH}_3\text{NH}_3\text{PbI}_3$  perovskite. Moreover the peaks are matched completely between the two measurements, suggesting that there is no change in the crystallographic structure of the perovskite over time, which indicates the high stability of these hole conductor free perovskite solar cells. Figure 6B shows the reproducibility for of the  $\text{CH}_3\text{NH}_3\text{PbI}_3/\text{TiO}_2$  heterojunction solar cells made using the optimum conditions describe above ( $\text{TiO}_2$  thickness, wait time, blocking layer condition). More than 45% of the cells show efficiencies above 8%, while more than 11% show efficiencies above 10%. The average power conversion efficiency is 7.7%.



**Figure 6:**(A) XRD diffraction of fresh cell and the same cell after a month. About two third of the peaks belong to the Orthorhombic structure of the  $\text{CH}_3\text{NH}_3\text{PbI}_3$  perovskite, while one third belongs to the tetragonal structure of the  $\text{CH}_3\text{NH}_3\text{PbI}_3$  perovskite. (B) Histogram of the  $\text{CH}_3\text{NH}_3\text{PbI}_3/\text{TiO}_2$  heterojunction solar cells efficiency. The average efficiency is 7.7%, with more than 11% of the cells show efficiencies above 10%.

Using the optimum conditions discussed in this paper, our best cells achieved PCE of 10.85% with  $V_{oc}$  of 0.84V, FF of 68% and  $J_{sc}$  of  $19 \text{ mA/cm}^2$ . Its current density-voltage curve is presented in figure 7A. The corresponding IPCE spectra is shown in figure 7B, it reaches its maximum of 88% at 400nm-600nm wavelengths and gradually drops at longer wavelength corresponding to its absorption spectrum. Without a hole conductor the charge carrier at the gold back contact aren't extracted efficiently, which influence the carrier collection at longer wavelength (explains the decrease in the IPCE spectra from 600nm wavelength). The integration of the IPCE spectra gives current density of  $18.3 \text{ mA/cm}^2$  as shown in figure 7B, there is good agreement with the current density measured by the solar simulator. To the best of our knowledge, this is the highest efficiency reported for  $\text{CH}_3\text{NH}_3\text{PbI}_3$  perovskite based solar cells without a hole transport material.



**Figure 7:**(A) current density-voltage curve of the champion hole conductor free  $\text{CH}_3\text{NH}_3\text{PbI}_3/\text{TiO}_2$  heterojunction solar cell; (B) The corresponding IPCE spectrum and its integrated current density.

## Conclusions

This work describes an in-depth study of the parameters influencing the PV performance of hole conductor free lead halide iodide solar cells. A two-step deposition technique of the perovskite was used, which assisted in achieving higher efficiencies. We have found a correlation between the depletion region width at the  $\text{TiO}_2/\text{CH}_3\text{NH}_3\text{PbI}_3$  junction and the efficiency observed. The highest efficiency was achieved when half of the  $\text{TiO}_2$  film was depleted. It was observed from the XRD analysis that the crystallographic structure does not change over time which supports the high stability of these cells. The best PCE achieved in this study was 10.85% which is, to date, the highest efficiency of these hole conductor free perovskite solar cells.

## Experimental

### Method and device fabrication

CH<sub>3</sub>NH<sub>3</sub>I was synthesized as described earlier<sup>5</sup> by reacting 30 mL of methylamine (40% in methanol, TCI) and 32.3 mL of hydroiodic acid (57 wt% in water, Aldrich) in a 250 mL round bottom flask at 0°C for 2h with stirring. The precipitate was recovered by putting the solution on a rotavap and carefully removing the solvents at 50°C. The yellowish raw product of methylammonium iodide (CH<sub>3</sub>NH<sub>3</sub>I) was washed with ethanol by stirring the mixture for 30 min. Then the mixture was filtered and washed with diethylether. The washing step was repeated three times. After filtration, the solid was collected and dried at 60°C in a vacuum oven for 24 h.

**Device fabrication:** The substrate of the device was a SnO<sub>2</sub>:F(FTO) conducting glass (15Ω · cm<sup>-1</sup>, Pilkington). A blocking layer was deposited on the FTO glass using a solution of titanium diisopropoxidebis(acetylacetonate)(TiDIP, 75% in isopropanol, Aldrich) in ethanol. Various volumetric ratios (0.05%, 0.10%, 0.15%, 0.20%) of the TiDIP solution were spin coated and then annealed at 450°C for 35 min. Various dilutions of Titania paste (20nm, Dyesol) were prepared by diluting the titania paste with ethanol at different weight ratios. The TiO<sub>2</sub> solution was spin coated and annealed at 500°C for 30 min subsequent to TiCl<sub>4</sub> treatment for 30 min at 70°C and annealing at 500°C for 30 min.

The synthesis of CH<sub>3</sub>NH<sub>3</sub>PbI<sub>3</sub> on the TiO<sub>2</sub> surface was carried out by a two-step deposition technique as described previously<sup>18</sup> but with several modifications. At the beginning, PbI<sub>2</sub> was dropped onto the TiO<sub>2</sub> film and spin coated after various wait time periods (1 min, 1.5 min, 3 min, or 5min) followed by annealing at 70°C for 30 min. In the second step, the cell was dipped into 10mg/ml of CH<sub>3</sub>NH<sub>3</sub>I solution at 70°C for 20 sec, and then annealed at 70°C for another 30 min. During the dip and the annealing, the CH<sub>3</sub>NH<sub>3</sub>PbI<sub>3</sub> was formed, indicated by the dark brown color of the electrode. Finally, the back contact was deposited by evaporating 50nm of gold under pressure of 5\*10<sup>-6</sup>Torr. The active area was 0.09 cm<sup>2</sup>.

**Profiler** – the thickness measurements of the TiO<sub>2</sub> films were performed by Veeco Dektak 150 profiler.

**Extra High Resolution Scanning Electron Microscopy (XHR-SEM)** – Magellan XHR SEM was performed with FEI (Field Emission Instruments), The Netherlands. The measurement conditions were 5 kV at a magnification of 100,000.

**X-ray diffraction** – X-ray powder diffraction measurements were performed in grazing incidence X-ray diffraction (GIXRD) mode on the D8 Advance diffractometer (Bruker AXS, Karlsruhe, Germany) with a goniometer radius of 217.5 mm, a secondary graphite monochromator, 2° Soller slits and a 0.2 mm receiving slit. XRD patterns within the range  $5^\circ$  to  $60^\circ 2\theta$  were recorded at room temperature using CuK $\alpha$  radiation ( $1.5418 \text{ \AA}$ ) with the following measurement conditions: tube voltage of 40 kV, tube current of 40 mA, step-scan mode with a step size of  $0.02^\circ 2\theta$  and counting time of 1–3 s per step. The value of the grazing incidence angle was  $2.5^\circ$ .

**Photovoltaic characterization** – Photovoltaic measurements were made on a New Port system, composed of Oriel I–V test station using an Oriel Sol3A simulator. The solar simulator is class AAA for spectral performance, uniformity of irradiance, and temporal stability. The solar simulator is equipped with a 450 W xenon lamp. The output power is adjusted to match AM1.5 global sunlight ( $100 \text{ mWcm}^{-2}$ ). The spectral match classifications are IEC60904-9 2007, JIC C 8912, and ASTM E927-05. I–V curves were obtained by applying an external bias to the cell and measuring the generated photocurrent with a Keithley model 2400 digital source meter. The voltage step and delay time of photocurrent were 10 mV and 40 ms, respectively. Oriel IQE-200 was used to determine the monochromatic incident photon-to-electric current conversion efficiency. Under full computer control, light from a 150 W xenon arc lamp was focused through a monochromator in the 300–1800 nm wavelength range onto the photovoltaic cell under test. The monochromator was incremented through the visible spectrum to generate the IPCE ( $\lambda$ ) as defined by  $\text{IPCE}(\lambda) = 12,400 (J_{sc}/\lambda \phi)$ , where  $\lambda$  is the wavelength,  $J_{sc}$  is the short-circuit photocurrent density ( $\text{mA cm}^{-2}$ ), and  $\phi$  is the incident radiative flux ( $\text{mWcm}^{-2}$ ). Photovoltaic performance was measured by using a metal mask with an aperture area of  $0.09 \text{ cm}^2$ .

**Capacitance voltage measurements** – The measurements were performed using a Metrohm Autolab system, equipped with a PGTSTAT302N potentiostat instrument. The frequency was 1 kHz at bias potentials between 0 and 0.9 V.

### Acknowledgments

We would like to thank the Israel Alternative Energy Foundation (I-SAEF) that financed this research. We would like to thank Dr. Vladimir Uvarov and Ms. Evgenia Blayvas from the Harvey M. Krueger Center for Nanoscience and Nanotechnology at the Hebrew University for the XRD and the HR-SEM measurements, respectively.

## References

- <sup>1</sup> Akihiro Kojima; Masashi Ikegami; Kenjiro Teshima; and Tsutomu Miyasaka. Highly Luminescent Lead Bromide Perovskite Nanoparticles Synthesized with Porous Alumina Media *Chem. Lett.* **2012**, 41, 397.
- <sup>2</sup> C.R. Kagan ; D. B. Mitzi ; C. D. Dimitrakopoulos. Organic-Inorganic Hybrid Materials as Semiconducting Channels in Thin-Film Field-Effect Transistors. *Science*, **1999**, 286, 945.
- <sup>3</sup> D.B Mitzi ; C.A. Feild ; Z. Schlesinger ; R.B. Laibowitz. Transport Optical and Magnetic properties of the conducting Halide Perovskite  $\text{CH}_3\text{NH}_3\text{SnI}_3$ . *J.Solid State Chem.* **1995**, 114, 159.
- <sup>4</sup> Akihiro Kojima; Kenjiro Teshima; Yasuo Shirai; Tsutomu Miyasaka. Organometal Halide Perovskites as Visible-Light Sensitizers for Photovoltaic Cells. *J.Am. Chem. Soc.* **2009**, 131, 6050–6051.
- <sup>5</sup> Jeong-Hyoek Im; Jaehoon Chung; Seung-Joo Kim; Nam-Gyu Park. Synthesis, structure, and photovoltaic property of a nanocrystalline 2H perovskite-type novel sensitizer  $(\text{CH}_3\text{CH}_2\text{NH}_3)\text{PbI}_3$ , *Nanoscale Research Letters* **2012**, 7, 353.
- <sup>6</sup> Jeong-Hyeok Im; Chang-Ryul Lee; Jin-Wook Lee; Sang-Won Park; Nam-Gyu Park. 6.5% efficient perovskite quantum-dot-sensitized solar cell. *Nanoscale*. **2011**, 3, 4088.
- <sup>7</sup> H.-S. Kim, C.-R. Lee, J.-H. Im, K.-B. Lee, T. Moehl, A. Marchioro, S.-J. Moon, R. Humphry-Baker, J.-H. Yum, J. E. Moser, M. Grätzel, Nam-Gyu Park . Lead Iodide Perovskite Sensitized All-Solid-State Submicron Thin Film Mesoscopic Solar Cell with Efficiency Exceeding 9%. *Nature Scientific Reports* **2012**, 2, 591.
- <sup>8</sup> Chung, I.; Lee, B.; He, J.; Chang, R. P. H.; Kanatzidis, M. G. All-solid-state dye-sensitized solar cells with high efficiency. *Nature* **2012**, 485, 486-489.
- <sup>9</sup> Lee, M.; Teuscher, M. J.; Miyasaka, T.; Murakami, T. N.; Snaith, H. J. Efficient Hybrid Solar Cells Based on Meso-Superstructured Organometal Halide Perovskites. *Science* **2012**, 338, 643-644.
- <sup>10</sup> James M. Ball, Michael M. Lee, Andrew Hey and Henry J. Snaith, Low-temperature processed meso-superstructured to thin-film perovskite solar cells, *Energy & Environmental Science*, **2013**, DOI: 10.1039/c3ee40810h.
- <sup>11</sup> Jin Hyuck Heo, Sang Hyuk Im, Jun Hong Noh, Tarak N. Mandal, Choong-Sun Lim, Jeong Ah Chang, Yong Hui Lee, Hi-jung Kim, Arpita Sarkar, Md. K. Nazeeruddin, Michael Grätzel & Sang Il Seok, Efficient inorganic-organic hybrid heterojunction solar cells containing perovskite compound and polymeric hole conductors, *Nature Photonics* **2013**, 7, 486-491.
- <sup>12</sup> Bing Cai, Yedi Xing, Zhou Yang, Wen-Hua Zhang and Jieshan Qiu, High performance hybrid solar cells sensitized by organolead halide perovskites, *Energy Environ. Sci.*, **2013**, 6, 1480.
- <sup>13</sup> Eran Edri, Saar Kirmayer, David Cahen, and Gary Hodes, High Open-Circuit Voltage Solar Cells Based on Organic-Inorganic Lead Bromide Perovskite, *J.Phys. Chem. Lett.* **2013**, DOI: 10.1021/jz400348q.
- <sup>14</sup> Hui-Seon Kim, Ivan Mora-Sero, Victoria Gonzalez-Pedro, Francisco Fabregat-Santiago, Emilio J. Juarez-Perez, Nam-Gyu Park & Juan Bisquert, Mechanism of carrier accumulation in perovskite thin-absorber solar cells, *Nature communications*, **2013**, DOI: 10.1038/ncomms3242.
- <sup>15</sup> Edoardo Mosconi, Anna Amat, Md.K.Nazeeruddin, Michael Grätzel, and Filippo De Angelis, First-Principles Modeling of Mixed Halide Organometal Perovskites for Photovoltaic Applications, *J. Phys. Chem. C* **2013**, 117, 13902–13913
- <sup>16</sup> Samuel D. Stranks, Giles E. Eperon, Giulia Grancini, Christopher Menelaou, Marcelo J. P. Alcocer, Tomas Leijtens, Laura M. Herz, Annamaria Petrozza, Henry J. Snaith, Electron-Hole Diffusion Lengths Exceeding 1 Micrometer in an Organometal Trihalide Perovskite Absorber,



*Science* **2013**, 342, 341.

<sup>17</sup> Guichuan Xing, Nripan Mathews, Shuangyong Sun, Swee Sien Lim, Yeng Ming Lam, Michael Grätzel, Subodh Mhaisalkar, Tze Chien Sum, Long-Range Balanced Electron- and Hole-Transport Lengths in Organic-Inorganic  $\text{CH}_3\text{NH}_3\text{PbI}_3$ , *Science* **2013**, 342, 344.

<sup>18</sup> Julian Burschka, Norman Pellet, Soo-Jin Moon, Robin Humphry-Baker, Peng Gao, Mohammad K. Nazeeruddin & Michael Grätzel, Sequential deposition as a route to high-performance perovskite-sensitized solar cells, *Nature*, **2013**, 499, 316.

<sup>19</sup> Mingzhen Liu, Michael B. Johnston, Henry J. Snaith, Efficient planar heterojunction perovskite solar cells by vapour deposition, *Nature*, **2013**, doi:10.1038/nature 12509.

<sup>20</sup> Etgar, L.; Gao, P.; Xue, Z.; Peng, Q.; Chandiran, A. K.; Liu, B.; Nazeeruddin, Md.K.; Grätzel, M. Mesoscopic  $\text{CH}_3\text{NH}_3\text{PbI}_3/\text{TiO}_2$  Heterojunction Solar Cells. *J. Am. Chem. Soc.* **2012**, 134, 17396–17399.

<sup>21</sup> Walleed Abu Laben, Lioz Etgar. Depleted hole conductor-free lead halide iodide heterojunction solar cell, *Energy Environ. Sci.*, **2013**, DOI:10.1039/C3EE42282H.

<sup>22</sup> Jiangjian Shi, Juan Dong, Songtao Lv, Yuzhuan Xu, Lifeng Zhu, Junyan Xiao, Xin Xu, Huijue Wu, Dongmei Li, Yanhong Luo, and Qingbo Meng *Appl. Phys. Lett.* **2014**, 104, 063901;

<sup>23</sup> Schottky, W. Vereinfachte und Erweiterte Theorie der Randschicht-Gleichrichter. *Z. Phys.* **1942**, 118, 539–592.

<sup>24</sup> J. P. Clifford, K. W. Johnston, L. Levina, and E. H. Sargent, Schottky barriers to colloidal quantum dot films, *Appl. Phys. Lett.* **2007**, 91, 253117.

<sup>25</sup> A. Poglitsch and D. Weber, Dynamic disorder in methylammonium trihalogenoplumbates (II) observed by millimeter-wave spectroscopy, *J. Chem. Phys.* **1987**, 87 (11).

<sup>26</sup> T. Baikie, Y. Fang, J. M. Kadro, M. Schreyer, F. Wei, S. G. Mhaisalkar, M. Graetzel and T. J. White *J. Synthesis and crystal chemistry of the hybrid perovskite  $(\text{CH}_3\text{NH}_3)\text{PbI}_3$  for solid-state sensitised solar cell applications, *Mater. Chem. A*, **2013**, 1, 5628–5641.*

<sup>27</sup> J. M. Luther, M. Law, M. C. Beard, Q. Song, M. O. Reese, R. J. Ellingson, and A. J. Nozik, Schottky Solar Cells Based on Colloidal Nanocrystal Films, *Nano Lett.*, **2008**, 8, (10), 3488–3492.

<sup>28</sup> B. O'Regan, J. Moser, M. Anderson, M. Graetzel, Vectorial. Vectorial electron injection into transparent semiconductor membranes and electric field effects on the dynamics of light-induced charge separation, *J. Phys. Chem.* **1990**, 94, 8720–8726.

<sup>29</sup> S. Nakade, Y. Saito, W. Kubo, T. Kanzaki, T. Kitamura, Wada, Y. S. Yanagida, Enhancement of electron transport in nano-porous  $\text{TiO}_2$  electrodes by dye adsorption, *Electrochem. Commun.* **2003**, 5, 804–808.

<sup>30</sup> A. Zaban, A. Meier, B. A. Gregg, Electric Potential Distribution and Short-Range Screening in Nanoporous  $\text{TiO}_2$  Electrodes, *J. Phys. Chem. B* **1997**, 101, 7985–7990.